ELSEVIER

Chemical Engineering Science 59 (2004) 5157–5165

Chemical Engineering Science

www.elsevier.com/locate/ces

Computational fluid dynamics for dense gas–solid fluidized beds: a multi-scale modeling strategy

M.A. van der Hoef*, M. van Sint Annaland, J.A.M. Kuipers

Department of Science and Technology, University of Twente, P.O. Box 217, 7500 AE Enschede, The Netherlands

Received 5 March 2004; accepted 4 July 2004
Available online 24 August 2004

Abstract

Dense gas–particle flows are encountered in a variety of industrially important processes for large scale production of fuels, fertilizers and base chemicals. The scale-up of these processes is often problematic, which can be related to the intrinsic complexities of these flows which are unfortunately not yet fully understood despite significant efforts made in both academic and industrial research laboratories. In dense gas–particle flows both (effective) fluid–particle and (dissipative) particle–particle interactions need to be accounted for because these phenomena, to a large extent, govern the prevailing flow phenomena, i.e. the formation and evolution of heterogeneous structures. These structures have significant impact on the quality of the gas–solid contact and as a direct consequence thereof strongly affect the performance of the process.

Due to the inherent complexity of dense gas-particles flows, we have adopted a multi-scale modeling approach in which both fluid–particle and particle–particle interactions can be properly accounted for. The idea is essentially that fundamental models, taking into account the relevant details of fluid–particle (lattice Boltzmann model (LBM)) and particle–particle (discrete particle model (DPM)) interactions, are used to develop closure laws to feed continuum models which can be used to compute the flow structures on a much larger (industrial) scale. Our multi-scale approach (see Fig. 1) involves the LBM, the DPM, the continuum model based on the kinetic theory of granular flow, and the discrete bubble model. In this paper we give an overview of the multi-scale modeling strategy, accompanied by illustrative computational results for bubble formation. In addition, areas which need substantial further attention will be highlighted.

Keywords: Fluidization; Multiphase flow; Simulation; Discrete particle model; CFD; Kinetic theory

1. Introduction

Dense gas–particle flows are frequently encountered in a variety of industrially important gas–solid contactors, of which the gas-fluidized bed can be mentioned as a very important example. Due to their favorable mass and heat transfer characteristics, gas-fluidized beds are often applied in the chemical, petrochemical, metallurgical, environmental and energy industries in large scale operations involving a.o. coating, granulation, drying, and synthesis of fuels and base chemicals (Kunii and Levenspiel, 1991). Lack of understanding of the fundamentals of dense gas–particle flows, and in particular of the effects of gas–particle drag and particle–particle interactions (Kuipers et al., 1998; Kuipers and van Swaaij, 1998), has led to severe difficulties in the scale-up of these industrially important gas–solid contactors (van Swaaij, 1990). To arrive at a better understanding of these complicated systems in which both gas–particle and particle–particle interactions play a dominant role, computer models have become an indispensable tool. However, the prime difficulty with modeling gas-fluidized beds is the large separation of scales: the largest flow structures can be of the order of meters; yet these structures are found to be directly influenced by details of the particle–particle collisions, which take place on the scale of millimeters or less. Therefore, we have adopted a multi-level modeling strategy (see Fig. 1), with the prime goal to (i) obtain a fundamental insight of the complex

* Corresponding author. Tel.: +31-534892953.
E-mail address: m.a.vanderhoef@utwente.nl (M.A. van der Hoef).

0009-2509/$ - see front matter © 2004 Elsevier Ltd. All rights reserved.
doi:10.1016/j.ces.2004.07.013

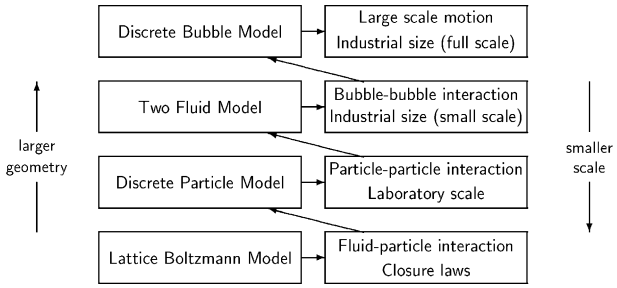

Fig. 1. Multi-level modeling scheme.

dynamic behavior of dense gas–particle fluidized suspensions; that is, to gain an understanding based on elementary *physical* principles such as drag, friction, dissipation etc., (ii) from this insight, develop models with *predictive* capabilities for dense gas–particle flows encountered in engineering scale equipment. To this end, we consider gas–solid flows at four distinctive levels of modeling.

At the most detailed level of description, the gas flow field is modeled at scales *smaller* than the size of the solid particles. The interaction of the gas phase with the solid phase is incorporated by imposing "stick" boundary conditions at the surface of the solid particles. This model thus allows us to measure the effective momentum exchange between the two phases, which can be used in the higher scale models. In our model, the flow field between the spheres is solved by the lattice Boltzmann model (LBM) (Succi, 2001; Ladd, 1993; Ladd and Verberg, 2001), although in principle other methods (such as standard computational fluid dynamics) could be used as well.

At the intermediate level of description, the flow field is modeled at a scale *larger* than the size of the particles, where a grid cell typically contains $O(10^2)$–$O(10^3)$ particles, which are furthermore assumed to be perfect spheres (diameter d). This model consists of two parts: a Lagrangian code for updating the positions and velocities of the solid particles from Newton's law, and an Eulerian code for updating the local gas density and velocity from the Navier–Stokes equation (Hoomans et al., 1996). The advantage of this model is that it can account for the particle wall and particle–particle interactions in a realistic manner, for system sizes of about $O(10^6)$ particles, which is sufficiently large to allow for a direct comparison with laboratory-scale experiments. As a logical consequence of this approach, a closure law for the effective momentum exchange has to be specified, which can be achieved on the basis of the aforementioned LB simulations. Note that in chemical engineering, to date mainly empirical relations are used for the friction coefficient β (defined by (5)), such as the Ergun correlation (Ergun, 1952) for porosities $\varepsilon < 0.8$:

$$\frac{\beta d^2}{\mu} = 150\,\frac{(1-\varepsilon)^2}{\varepsilon} + 1.75\,\frac{(1-\varepsilon)}{\varepsilon}Re \tag{1}$$

and the Wen and Yu equation (Wen and Yu, 1966) for porosities $\varepsilon > 0.8$:

$$\frac{\beta d^2}{\mu} = \tfrac{3}{4}\,C_d\,Re(1-\varepsilon)\varepsilon^{-2.65},$$
$$C_d = \begin{cases} 24(1+0.15Re^{0.687})/Re & Re < 10^3, \\ 0.44 & Re > 10^3, \end{cases} \tag{2}$$

where μ is the viscosity of the gas phase, Re is the Reynolds number, and C_d the drag coefficient, for which the expression of Schiller and Nauman (1935) is used.

At an even larger scale, a continuum description is employed for the solid phase, i.e. the solid phase is not described by individual particles, but by a local density and velocity field. Hence in this model, both the gas phase and the solid phase are treated on an equal footing, and for both phases an Eulerian code is used to describe the time evolution (see Kuipers et al. (1992) and Gidaspow (1994), amongst others). The information obtained in the two smaller-scale models is then included in the continuum models via the kinetic theory of granular flow. The advantage of this model is that it can predict the flow behavior of gas–solid flows at life-size scales, and these models are therefore widely used in commercial fluid flow simulators of industrial scale equipment.

Finally, at the largest scale, the (larger) bubbles that are present in gas–solid fluidized beds are considered as discrete objects, similar to the solid particles in the DPM. This model is an adapted version of the discrete bubble model (DBM) for gas–liquid bubble columns. We want to stress that this model—as outlined in Section 4—has been developed quite recently, and the results should be considered as very preliminary.

In this paper, we will give an overview of these four levels of modeling as they are employed in our research group. Our particular focus will be on the effect of the drag force—as obtained from the LB simulation—on the formation of bubbles in the higher scale models. In the following sections we will describe each of these models in more detail.

2. LBM

The LBM originates from the lattice-gas cellular automata (LGCA) models (Frisch et al., 1986) for simple fluids. The LGCA model is basically a discrete, simplified version of the molecular dynamics model, which involves propagations and collisions of particles on a lattice. LGCA models have proved a simple and efficient way to simulate a simple fluid at the microscopic level, where it has been demonstrated both numerically and theoretically that the resulting macroscopic flow fields obey the Navier–Stokes equation. The LBM is the ensemble averaged version of the LGCA model, so that it represents a propagation and collision of the particle *distributions* instead of the *actual* particles as in the LGCA models (Succi, 2001; McNamara and Zanetti, 1988). From a macroscopic point of view, the LBM can be regarded as a finite difference scheme that solves the Boltzmann equation,

the fundamental equation in kinetic theory which underlies of the equations of hydrodynamics. In its most simple form, the finite difference scheme reads

$$f(\vec{v},\vec{r}+\vec{v}\,\delta t,t+\delta t)-f(\vec{v},\vec{r},t) = -\frac{\delta t}{\tau}(f(\vec{v},\vec{r},t)-f^{\mathrm{eq}}(\vec{v},\vec{r},t)) \quad (3)$$

where f is the single particle distribution function, which is equivalent to the fluid density in the six-dimensional velocity-coordinate space, and f^{eq} represents the equilibrium distribution. In Eq. (3), the position $\vec{r}$ and velocity $\vec{v}$ are discrete, i.e. the possible positions are restricted to the sites of a lattice, and thus the possible velocities are vectors connecting nearest neighbor sites of this lattice. Note that Eq. (3) represents a propagation, followed by a "collision" (relaxation to the equilibrium distribution). From the single particle distribution function, the hydrodynamic variables of interest—the local gas density ρ and velocity $\vec{u}$—are obtained by summing out over all possible velocities:

$$\rho(\vec{r},t)=\sum_{\vec{v}} f(\vec{v},\vec{r},t),$$

$$\rho(\vec{r},t)\vec{u}(\vec{r},t)=\sum_{\vec{v}} \vec{v}\,f(\vec{v},\vec{r},t). \quad (4)$$

It can be shown that the flow fields obtained from the LBM are—to order δt^2—equivalent to those obtained from the Navier–Stokes equation, where the viscosity is set by the relaxation time τ. One of the advantages of the LBM over other finite difference models for fluid flow, is that boundary conditions can be modeled in a very simple way. This makes the method particularly suited to simulate large moving particles suspended in the fluid phase. An obvious choice of the boundary condition is where the gas next to the solid particle moves with the local velocity of the surface of the solid particle, i.e. the so-called "stick" boundary condition. For a spherical particle suspended in an infinite three-dimensional system, moving with velocity $\vec{v}$, this condition will give rise to a frictional force on the particle $\vec{F}=3\pi\mu d\vec{v}$, at least in the limit of low-particle Reynolds numbers $Re=\rho d\varepsilon v/\mu$, where d is the hydrodynamic diameter of the particle, and μ is the shear viscosity. A particular efficient and simple way to enforce stick boundary conditions for static particles in the LBM is to let the distributions "bounce back" at the boundary nodes (Ladd, 1993; Ladd and Verberg, 2001); these nodes are defined as the points halfway two lattice sites which are closest to the actual surface of the particle (see Fig. 2, left graph, solid squares). For non-static particles, the rules involve some simple modifications of the bounce back rule, depending on the local boundary velocity. For details we refer to Ladd (1993) and Ladd and Verberg (2001). In Fig. 2 (right graph), we show the LBM simulation result for the velocity of a single free falling sphere in an (effectively) unbounded fluid. As can be seen from Fig. 2, the boundary rules result in a terminal velocity according to the Stokes–Einstein friction force. Note that the actual plateau value of the velocity is slightly smaller than the theoretical prediction. This can be attributed to the fact that the diameter of the particle is not well-defined, due to the irregular shape of boundary-node surface of the sphere. In fact, the free falling sphere experiment (or a similar experiment with periodic boundary conditions) is used for calibration purposes, that is, the effective hydrodynamic diameter d of a sphere is obtained from its terminal velocity, where it isassumed that the Stokes–Einstein relation holds. It has been shown (Ladd, 1993) that this gas–solid model also produces accurate results for systems with more than one particle; for instance, the hydrodynamic force that two approaching spheres exert on each other is in perfect agreement with the analytical solution (Ladd, 1993). Note that the drag force F_d can also be directly measured in the simulation, from the change in gas momentum due to the boundary rules. To obtain the drag force in random arrays of particles at some given porosity, it is therefore more convenient to keep the spheres fixed to their positions, and let the gas flow past the spheres with constant velocity u_o, according to the desired Re number ($Re=\rho\varepsilon d u_o/\mu$). The average drag force $\langle F_d\rangle$ on a sphere then follows from the average change in gas momentum, from which the friction coefficient β can be obtained:

$$\beta=\frac{1-\varepsilon}{V_p}\frac{\langle F_d\rangle}{u_o}, \quad V_p=\tfrac{1}{6}\pi d^3. \quad (5)$$

By using this method, we found for low Reynolds number excellent agreement with data obtained by multipole expansion methods (van der Hoef et al., 2004). By contrast, it was found that the widely used empirical correlations (1) and (2) significantly underestimate the drag force, at least for low Reynolds numbers. In this paper, we want to present some preliminary results from the LBM for finite Reynolds numbers. In Fig. 3 we show our simulation data in a $(\beta d^2/\mu)(\varepsilon/(1-\varepsilon)Re)$ vs. $Re/(1-\varepsilon)$ graph. It was shown by Ergun (1952) that in such a representation, all experimental data falls onto a single curve (solid line in Fig. 3). We find that our LBM data deviates substantially from Ergun Eq. (1): for low Re numbers the Ergun equation

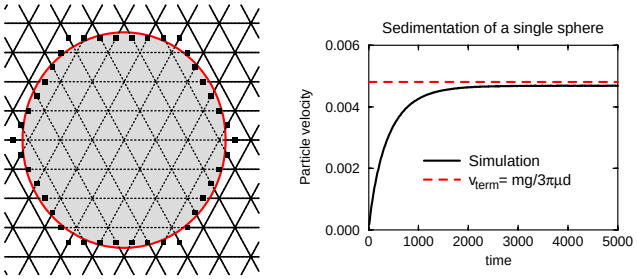

Fig. 2. Left graph: example of a boundary node map for a disc in a two-dimensional hexagonal lattice. Right graph: velocity of a single sphere in a three-dimensional LB gas. The black line is the data from LBM, which has the proper functional form $v(t)=v_\infty(1-\exp(-gt/v_\infty))$. The grey line is theoretical terminal velocity, which is slightly higher than v_∞.

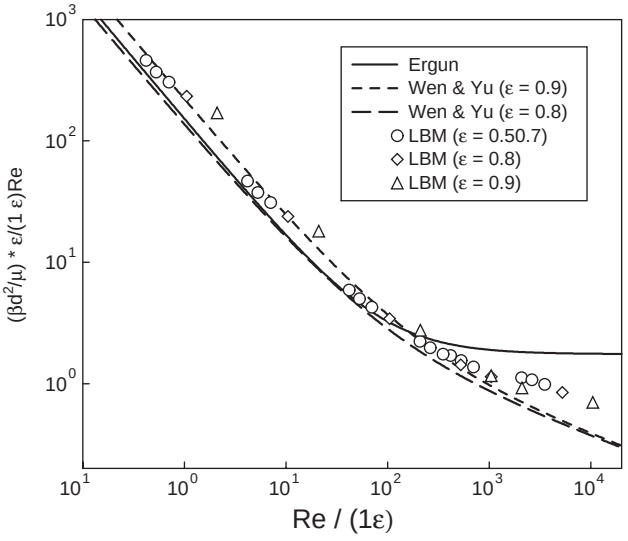

Fig. 3. Normalized drag force at arbitrary Reynolds numbers and gas fractions. The symbols represent the simulation data, the lines the empirical correlations.

underestimates the drag force, whereas for high *Re* numbers that Ergun equation overestimates the drag force. Simulations on binary systems (van der Hoef et al., 2004) showed that a possible cause of the discrepancy at lower Reynolds number could be that the experimental systems were not strictly monodisperse. Note also that the Ergun equation was derived for packed beds, and is not expected to be valid for high gas fractions. Our simulation data turns out to be in reasonable agreement with the expression by Hill et al. (2001a,b) which was fitted to LB simulation data of systems comparable to those that we have studied. On the basis of our data from the LB simulations, we suggest the following modification to the Ergun equation:

$$\frac{\beta d^2}{\mu} = [180 + C_0]\frac{(1-\varepsilon)^2}{\varepsilon} + [1.75 + C_1]\frac{(1-\varepsilon)}{\varepsilon}Re \qquad (6)$$

with

$$C_0 = \frac{18\varepsilon^3(1 + 1.5\sqrt{1-\varepsilon})}{(1-\varepsilon)}.$$

Our data indicates that C_1 can be well fitted to a polynomial in $1-\varepsilon$; at present, our best fit is $C_1 = -1.3 + 1.9(1-\varepsilon) - 1.6(1-\varepsilon)^2$, which we will use in the following sections. However, as mentioned before, these are preliminary results, and the coefficients might change slightly on the basis of more extensive data. Note that by taking the limit $\varepsilon = 1$, $Re \to \infty$, we find that Eq. (6) corresponds to a drag coefficient $C_d(\infty) = 0.6$, which is much closer to the Schiller and Nauman (1935) value (0.44), than both Hill et al. (1.09) and Ergun (2.3). An elaborate disscussion of the simulation procedure and validation of the data, as well as a detailed comparison with various other expressions from literature, will be published elsewhere (van der Hoef et al., 2004; Beetstra et al., 2004).

3. Discrete particle model (DPM)

The DPM is one level higher in the multi-scale hierarchy. The most important difference with the LBM is that now the size of the particles is *smaller* than the grid size which is used the solve the equations of motion of the gas phase. This means that for the interaction with the gas phase, the particles are simply point sources and sinks of momentum, where the finite volume of the particles only comes in via an average gas fraction in the drag force relations. A second (technical) difference with the LBM is that the evolution of the gas phase now follows from a finite difference scheme of the Navier–Stokes equation, rather than the Boltzmann equation. A complete description of the method can be found in Hoomans et al. (1996), however, we will briefly discuss some of the basic elements here. The DPM consists of two parts: a Lagrangian part for updating the positions and velocities of the solid particles, and an Eulerian part for updating the local gas density and velocity. In the Lagrangian part, the equation of motion of each particle i (velocity $\vec{v}_i$, mass m_i, volume V_i) is given by Newton's law

$$m_i \frac{\mathrm{d}\vec{v}_i}{dt} = m_i\vec{g} + \frac{V_i\beta}{(1-\varepsilon)}(\vec{u} - \vec{v}_i) - V_i\nabla p + \vec{F}_i^{pp} + \vec{F}_i^{pw}, \qquad (7)$$

where the RHS represents the total force acting on the particle. This includes external forces (the gravitational force $m_i\vec{g}$), interaction forces with the gas phase (drag force $\sim \beta(\vec{u} - \vec{v}_i)$ and pressure force $V_i\nabla p$), and finally the particle–particle forces $\vec{F}_i^{pp}$ and particle–wall forces $\vec{F}_i^{pw}$, which represents the collisions, and possible long-range attractions between the particles, and particles and walls, respectively.

There are—in principle—two ways to calculate the trajectories of the solid particles from Newton's law. In a time-driven numerical simulation, the new position $\vec{r}_i(t + \mathrm{d}t)$ and velocity $\vec{v}_i(t + \mathrm{d}t)$ are calculated from the values at time t, via a standard integration scheme for ODEs. Such type of simulation is in principle suitable for any type of interaction force between the particles. In an event-driven simulation, the interactions between the particles are considered instantaneous ("collisions"), and the systems evolve directly ("free flight") from nearest collision event to next-nearest collision event, etc. This method is efficient for low-density systems, however it is not suitable for dense-packed system, or systems with long-range forces.

In the Eulerian part of the code, the evolution of the gas phase is determined by the volume-average Navier–Stokes equations

$$\frac{\partial}{\partial t}(\varepsilon\rho) + \nabla\cdot\varepsilon\rho\vec{u} = 0, \qquad (8)$$

$$\frac{\partial}{\partial t}(\varepsilon\rho\vec{u}) + \nabla\cdot\varepsilon\rho\vec{u}\vec{u} = -\varepsilon\nabla p - \nabla\cdot\varepsilon\bar{\bar{\tau}} - \vec{S} + \varepsilon\rho\vec{g}, \qquad (9)$$

where $\bar{\bar{\tau}}$ is the usual stress tensor, which includes the coefficient of shear viscosity. Note that there is a full two-way coupling with the Lagrangian part, i.e., the reaction from drag and pressure forces on the solid particles is included in the momentum equation for the gas phase via a source term $\vec{S}$

$$\vec{S} = \frac{1}{V}\int \sum_i \frac{V_i \beta}{1-\varepsilon}(\vec{u} - \vec{v}_i)\delta(\vec{r} - \vec{r}_i)\,\mathrm{d}V. \tag{10}$$

Eqs. (8) and (9) are solved with a semi-implicit method for pressure-linked equations (SIMPLE-algorithm), with a time step that is in general an order of magnitude larger than the time step used to update the particle positions and velocities.

The strength of the DPM is that it allows to study the effect of the particle–particle interactions on the fluidization behavior. In the most detailed model of description, the interparticle contact forces includes normal and tangential repulsive forces (modeled by linear springs), and dissipative forces (modeled by "dash pots"), and tangential friction forces (Walton, 1993). A DPM simulation study by Hoomans et al. (1996) showed that the heterogeneous flow structures in dense gas-fluidized beds are partly due to the collisional energy dissipation. More recently, Li and Kuipers (2003) demonstrated that such flow structures are also strongly influenced by the degree of non-linearity of the particle drag with respect to the gas fraction ε. In this paper, we want to use the DPM to demonstrate the effect of the various drag force correlations on the bubble formation in gas-fluidized beds, and compare the results with our experimental observations. In the DPM simulations, we consider a system of 15 cm × 45 cm × 1.5 cm (w × h × d), where the bed height at minimum fluidization conditions is equal to 22 cm. The particles have a diameter of 2.5 mm, a density of 2526 kg/m^3, and a coefficient of restitution equal to 0.97. For the interparticle momentum exchange, we used (i) the "traditional" Ergun/Wen and Yu combination, i.e. Eq. (1) for $\varepsilon < 0.8$, and Eq. (2) for $\varepsilon > 0.8$; (ii) the drag force relations derived by Hill et al. (2001a,b); and (iii) the drag force relation (6) which was derived from our LB simulations. For comparison, we also performed the real experiment, on a pseudo-2D fluidized bed (15 cm × 100 cm × 1.5 cm (w × h × d)), initially kept at incipient fluidization conditions using a porous plate for homogeneous background fluidization and a central jet for bubble injection. Spherical glass beads of 2.5 mm diameter were used of different color, which were initially ordered in two separate layers to visualize the extent of mixing induced by the bubble. Pictures of the bed where the bubble was injected were taken with a high-speed (262 Hz) digital camera.

In Fig. 4 we show snapshots of the bubble, both from experiments (a), and from simulations (b, c, and d). We find that both the drag relations from Hill et al., and (6) predict a smaller bubble size, and a more pronounced "raining" of particles through the roof of the bubble, compared to the Ergun/Wen and Yu drag relations. As a result the interface between the bubble and the emulsion phase is much more diffuse. The conclusion on the basis of the visual inspection of the bubble is that the drag relations derived from the LB simulations yield a better agreement with the experimental observations than the Ergun/Wen and Yu drag relations. In a more detailed analysis (Bokkers et al., 2004a), it was found that also the experimental particle velocity profiles were in reasonable agreement with the velocity profiles obtained from DPM simulations using the drag relations of Hill et al.

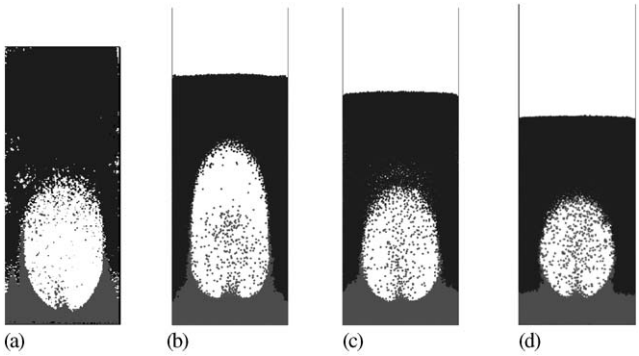

Fig. 4. Snapshots of the bubble in a mono-disperse fluidized bed 0.3 s after injection. (a) Experiment; (b) DPM simulation with Ergun/Wen and Yu; (c) DPM simulation with the drag relation from Hill et al. (2001a,b); (d) DPM simulation with the drag relation (6).

4. Two-fluid model (TFM)

The maximum number of particles that can be simulated with the DPM, as described in the previous section, is typically less than a million, whereas the number of particles that are present in an industrial size fluidized bed can be two to three *orders* of magnitude higher. Since both the CPU time and the required memory scales linear with the number of particles, it is obvious that DPM simulations of industrial size fluidized beds are beyond the capability of commercially available computer facilities within the foreseeable future. Therefore, a different type of model is used for simulations at larger scales, where the concept of a solid phase consisting of individual, distinguishable particles is abandoned. This so-called TFM describes both the gas phase and the solid phase as fully inter-penetrating continua, using a set of generalized Navier–Stokes equations (Kuipers et al., 1992; Gidaspow, 1994). That is, the time evolution of the gas phase is still governed by (8) and (9); for the solid phase, the discrete particle part (7) is now replaced by a set of continuous equations of the same form as (8) and (9):

$$\frac{\partial}{\partial t}(\varepsilon_s \rho_s) + \nabla \cdot \varepsilon_s \rho_s \vec{v} = 0, \tag{11}$$

$$\frac{\partial}{\partial t}(\varepsilon_s \rho_s \vec{v}) + \nabla \cdot \varepsilon_s \rho_s \vec{v}\vec{v} = -\varepsilon_s \nabla p - \nabla p_s - \nabla \cdot \varepsilon_s \bar{\bar{\tau}}_s + \vec{S} + \varepsilon_s \rho_s \vec{g} \tag{12}$$

with ρ_s, $\vec{v}$ and $\varepsilon_s = 1 - \varepsilon$ the local density, velocity, and volume fraction of the solid phase, respectively. In this description, the source term $\vec{S}$ is slightly different from (10), namely

$$\vec{S} = \beta(\vec{u} - \vec{v}). \tag{13}$$

Obviously, the numerical scheme for updating the solid phase is now completely analogous to (and synchronous with) that of the gas phase. Since the concept of particles has disappeared completely in such a modeling, the effect of particle–particle interactions can only be included indirectly, via an effective solids pressure and effective solids viscosity. A description which allows for a slightly more detailed description of particle–particle interactions follows from the kinetic theory of granular flow (KTGF); such theory expresses the diagonal and off-diagonal elements of the solids stress tensor (i.e. the solids pressure and solids shear rate) as a function of the granular temperature, defined as

$$\theta = \tfrac{1}{3}\langle \vec{C}_p \cdot \vec{C}_p \rangle, \tag{14}$$

where $\vec{C}_p$ represents the particle fluctuation velocity. The time evolution of the granular temperature itself is given by

$$\frac{3}{2}\left[\frac{\partial}{\partial t}(\varepsilon_s \rho_s \theta) + \nabla \cdot (\varepsilon_s \rho_s \theta \vec{v})\right] = -(p_s \overline{\overline{I}} + \varepsilon_s \overline{\overline{\tau}}_s) : \nabla \vec{v} - \nabla \cdot (\varepsilon_s \vec{q}_s) - 3\beta\theta - \gamma \tag{15}$$

with $\vec{q}_s$ the kinetic energy flux, and γ the dissipation of kinetic energy due to inelastic particle collisions. In Eqs. (11)–(15), there are still a number of unknown quantities (pressure, stress tensor, energy flux), which must be expressed in terms of the basic hydrodynamic variables (density, velocity, temperature), in order to get a closed set of equations. The derivation of such constitutive equations follows from the KTGF, and can be found in the books by Chapman and Cowling (1970) and Gidaspow (1994), and the papers by Jenkins and Savage (1983), Ding and Gidaspow (1990). In this work, the constitutive equations developed by Nieuwland et al. (1996) have been used for the particle phase rheology.

It will be interesting to show how this model will predict the bubble formation, compared to the more detailed DPM simulations. As in those simulations, we focus on the bubble size of a single bubble, injected in a mono-disperse fluidized bed at 0.2 s after injection. The dimensions and characteristics of the bed is similar as described in Section 3, only the bed is slightly higher (60 cm compared to 45 cm in the DPM simulations). In Fig. 5, we compare the results from the TFM simulations with the DPM simulation results from Section 3, and the experimental findings. Note that the solid phase is not represented by discrete particles ("dots") as in Fig. 4, but via a grey scale, indicating the local level of ε_s. As can be seen from Fig. 5, both the drag model from Hill, Koch and Ladd, and from this work (6), predicts a smaller bubble size and again a more pronounced "raining" of the particles through the roof of the bubble compared to the drag model by Ergun/Wen and Yu for both the DPM (compare snapshots (b) and (c)) and the TFM (compare (d) and (e)) results (Bokkers et al., 2004a). The bubble size is mainly determined by the drag exerted on the particles by the gas phase, whereas the mixing of the particles is dominated by particle–particle interactions, especially in the dense regions where sustained multi-particle contacts prevail (friction). A detailed study (Bokkers et al., 2004b) of the bed after a single bubble has passed showed that the TFM largely overpredicts the extent of solids mixing, i.e. the upward transportation of the bottom layer of particles. With the Ergun/Wen and Yu drag closures both the DPM and the TFM predict a slightly higher particle mixing due to the small overprediction of the bubble size.

5. Discrete bubble model (DBM)

Although the two-fluid model can simulate fluidized beds at a life-size scales, the largest scale industrial fluidized bed reactors (diameter 5 m, height 16 m) are still beyond its capabilities. However, it is possible to introduce yet another upscaling by considering the bubbles, as observed in the DPM and TFM models of gas-fluidized beds, as discrete entities. This is the so-called DBM, which has been succesfully applied in the field of gas–liquid bubble columns (Delnoij et al., 1997). However, the idea to apply this model to describe the large scale solids circulation that prevail in gas–solid reactors is new. In this paper, we want to show some first results of the DBM applied to gas–solid systems, which involves some slight modifications of the equivalent model for gas–liquid systems. To this end, the emulsion phase is modeled as a continuum—like the liquid in a gas–liquid bubble column—and the larger bubbles are treated as discrete bubbles. Note that granular systems have no surface tension, so in that respect there is a pronounced difference with the bubbles present in gas–liquid bubble columns. For instance, the gas will be free to flow through a bubble in the gas–solid systems, which is not the case for gas–liquid systems. As far as the numerical part is concerned, the DBM strongly resembles the DPM as outlined in Section 3, since it is also of the Euler–Lagrange type with the emulsion phase described by the volume-average Navier–Stokes equations

$$\frac{\partial}{\partial t}(\varepsilon\rho) + \nabla \cdot \varepsilon\rho\vec{u} = 0, \tag{16}$$

$$\frac{\partial}{\partial t}(\varepsilon\rho\vec{u}) + \nabla \cdot \varepsilon\rho\vec{u}\vec{u} = -\varepsilon\nabla p - \nabla \cdot \varepsilon\overline{\overline{\tau}} - \vec{S} + \varepsilon\rho\vec{g} \tag{17}$$

whereas the discrete bubbles are tracked individually according to Newton's second law of motion

$$m_b \frac{\mathrm{d}\vec{v}_b}{\mathrm{d}t} = \vec{F}_{\mathrm{tot}}, \tag{18}$$

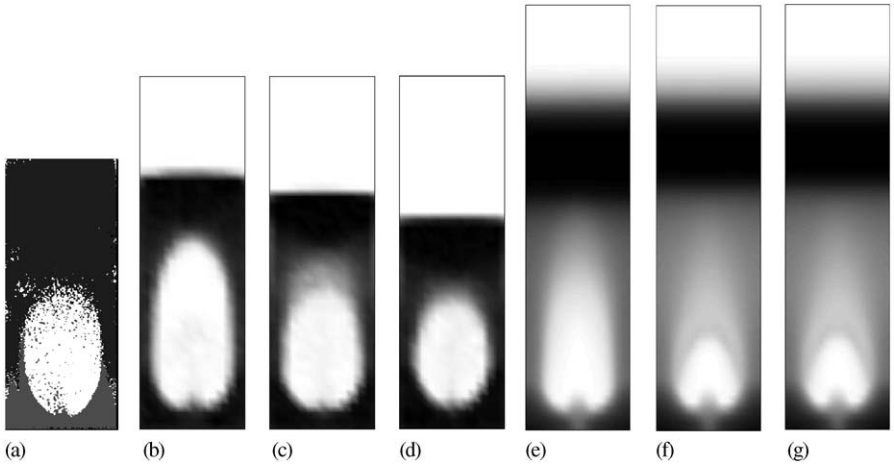

Fig. 5. Snapshots of the bubble in a mono-disperse fluidized bed at 0.2 s after injection: comparison between TFM with DPM and experiments; (a) experiment; (b) DPM with Ergun/Wen and Yu; (c) DPM with Hill, Koch and Ladd; (d) DPM with relation (6); (e) TFM with Ergun/Wen and Yu; (f) TFM with Hill, Koch and Ladd; (g) TFM with (6).

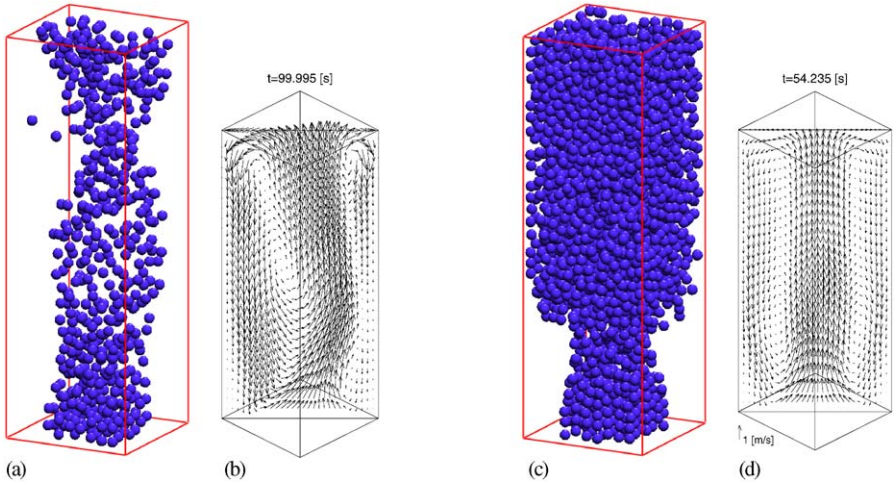

Fig. 6. Snapshots of the bubble hold-up in the DBM without coalescence, and the time average vector plot of the emulsion phase after 100 s of simulation; (a) + (b) $u_0 = 0.1\,\mathrm{m/s}$, $d_b = 0.04\,\mathrm{m}$; (c) + (d) $u_0 = 0.3\,\mathrm{m/s}$, $d_b = 0.04\,\mathrm{m}$.

where F_{tot} is the sum of different forces acting on a single bubble

$$\vec{F}_{\mathrm{tot}} = \vec{F}_g + \vec{F}_d + \vec{F}_p + \vec{F}_L + \vec{F}_{VM}. \tag{19}$$

As in the DPM, the total force on the bubble has contributions from gravity ($\vec{F}_g$), pressure gradients ($\vec{F}_p$) and drag from the interaction with emulsion phase ($\vec{F}_d$). For the drag force on a single bubble (diameter d_b), the correlations for the drag force on a single sphere are used, only with a modified drag coefficient C_d, such that it yields the Davies–Taylor relation $v_{br} = 0.711\sqrt{gd_b}$ for the rise velocity of a single bubble. Note that in (19), there are two forces present which are not found in the DPM, namely the lift force $\vec{F}_L$ and the virtual mass force $\vec{F}_{VM}$. The lift force is neglected in this application, whereas the virtual mass force coefficient is set to 0.5. An advantage of this approach to model large scale fluidized bed reactors is that the behavior of bubbles in fluidized beds can be readily incorporated in the force balance of the bubbles. In this respect, one can think of the rise velocity, and the tendency of rising bubbles to be drawn towards the center of the bed, from the mutual interaction of bubbles and from wall effects (Kobayashi et al., 2000). Coalescence, which is an highly prevalent phenomenon in fluidized beds, can also be easily included in the DBM, since all the bubbles are tracked individually.

With the DBM, two preliminary calculations have been performed for industrial scale gas-phase polymerization reactors, in which we want to demonstrate the effect of the superficial gas velocities, set to 0.1 and 0.3 m/s. The geometry of the fluidized bed was $1.0 \times 3.0 \times 1.0\,\mathrm{m}$ (w × h × d). The emulsion phase has a density of $400\,\mathrm{kg/m^3}$ and the apparent viscosity was set to 1.0 Pa s. The density of the bubble phase was $25\,\mathrm{kg/m^3}$. The bubbles were injected via 49 noz-

zles positioned equally distributed in a square in the middle of the column. In Figs. 6a and c snapshots are shown of the bubbles that rise in the fluidized bed with a superficial gas velocity of 0.1 and 0.3 m/s, respectively. It is clearly shown that the bubble hold-up is much larger with a superficial gas velocity of 0.3 m/s. However, the number of bubbles in this case might be too large, since coalescence has not been taken into account in these simulations. In Figs. 6b and d, time-averaged plots are shown of the emulsion velocity after 100 s of simulation. The large convection patterns, upflow in the middle, and downflow along the wall, and the effect of the superficial gas velocity, is clearly demonstrated. Future work will be focused on the implementation of closure equations in the force balance, like empirical relations for bubble rise velocities and the interaction between bubbles. The model can be augmented with energy balances to study temperature profiles in combination with the large circulation patterns.

6. Summary and outlook

In this paper, we have presented an overview of the multi-scale methods that we use to study gas–solid-fluidized beds. The key idea is that the methods at the smaller, more detailed scale can provide qualitative and quantitative information which can be used in the higher scale models. A typical example of such qualitative information is the insight (from the DPM simulations) that inelastic collisions and nonlinear drag can lead to heterogeneous flow structures. Even more important, however, is the *quantitative* information that the smaller scale models can provide. A typical example of this is the drag force relation obtained from the LBM simulations, which finds its direct use in both the DPM and TFM simulations. We should note here that although the new drag force relations seems to give results at the DPM/TFM level which compare better with the experimental findings, these relations are still far from optimal. In particular, it should be borne in mind that these drag force relations are derived for static, unbounded, homogeneous arrays of mono-disperse spheres. Yet, at the DPM/TFM level these relations are applied to systems which are—even locally—inhomogeneous and non-static; furthermore, rather ad-hoc modifications are used to allow for polydispersity. In future work, we want to focus on developing drag force relations for systems which deviate from the ideal conditions, where the parameters which would quantify such deviation may be trivial to define (polydispersity: width of the size distribution; moving particles: granular temperature) or not so trivial (inhomogeneities). Our LB results for the drag force in binary systems (van der Hoef et al., 2004) revealed significant deviations with the ad-hoc modifications of the monodisperse drag force relations, in which it is assumed that the drag force scales linearly with the particle diameter.

At present, mainly qualitative information from the DPM simulations is obtained, such as the aforementioned heterogeneous flow structures, which is caused by dissipative forces. Another example is the functional form of the velocity distribution. It was found that dissipative interaction forces cause an anisotropy in the distribution, although the functional form remains close to Gaussian for all three directions (Goldschmidt et al., 2002). It would be interesting to include the effect of anisotropy at the level of the TFM, for instance along the lines of the kinetic theory developed by Jenkins and Richman (1988) for shearing granular flows.

Although the continuum models have been studied extensively in the literature (e.g. Kuipers et al., 1992; Gidaspow, 1994), these models still lack the capability of describing quantitatively particle mixing and segregation rates in multi-disperse fluidized beds. An important improvement in the modeling of life-size fluidized beds could be made if direct quantitative information from the discrete particle simulations could find its way in the continuum models. In particular, it would be of great interest to find improved expressions for the solid pressure and the solid viscosity, as they are used in the TFM, however, it is a non-trivial task to extract direct data on the solid viscosity and pressure in a DPM simulation. A very simple, indirect method for obtaining the viscosity is to monitor the decay of the velocity of a large spherical intruder in the fluidized bed. The viscosity of the bed follows then directly from the Stokes–Einstein formula for the drag force. Very preliminary results—obtained from data of a high velocity impact—were in reasonable agreement with the experimental values for the viscosity. More elaborate simulations of these systems are currently underway. Finally, the DBM applied to gas–solid systems seems to be a promising new approach for describing the large-scale motion in life-size chemical reactors. Essential for this model to be successful is that reliable information with regard to rise velocities and mutual interaction of the bubbles is incorporated, which can be obtained from the lower scale simulations. In particular, the TFM and DPM simulations will be used to guide the formulation of additional rules to describe the coalescence of bubbles properly, which is at present not incorporated in the model. This will be the subject of future research.

Acknowledgements

The lattice Boltzmann simulations have been performed with the SUSP3D code developed by Anthony Ladd. We would like to thank him for making his code available, and Albert Bokkers for performing the DPM, TFM and DBM simulations.

References

Beetstra, R., van der Hoef, M.A., Kuipers, J.A.M., 2004. Lattice Boltzmann simulations of moderate Reynolds number flow past mono- and bidisperse arrays of spheres, to be submitted to Chemical Engineering Science.

Bokkers, G.A., Van Sint Annaland, M., Kuipers, J.A.M., 2004a. Mixing and segregation in a bidisperse gas–solid fluidised bed: a numerical and experimental study. Powder Technology 140, 176–186.

Bokkers, G.A., Van Sint Annaland, M., Kuipers, J.A.M., 2004b. In: Arena, U., Chirone, R., Miccio, M., Salatino, P. (Eds.), Proceedings of the 11th International Conference on Fluidization, 9–14 May 2004, Ischia, Italy, pp. 184–194.

Chapman, S., Cowling, T.G., 1970. The Mathematical Theory of Non-uniform Gases. third ed. Cambridge University Press, Cambridge.

Delnoij, E., Kuipers, J.A.M., van Swaaij, W.P.M., 1997. Computational fluid dynamics applied to gas–liquid contactors. Chemical Engineering Science 52, 3623. Ph.D. Thesis, University of Twente, Enschede, The Netherlands.

Ding, J., Gidaspow, D., 1990. A bubbling fluidization model using kinetic theory of granular flow. A.I.Ch.E. Journal 36, 523.

Ergun, S., 1952. Fluid flow through packed columns. Chemical Engineering Proceedings 48, 89.

Frisch, U., Hasslacher, B., Pomeau, Y., 1986. Lattice gas automata for the Navier–Stokes equation. Physical Review Letters 56, 1505.

Gidaspow, D., 1994. Multiphase Flow and Fluidization: Continuum and Kinetic Theory Descriptions. Academic Press, Boston.

Goldschmidt, M.J.V., Beetstra, R., Kuipers, J.A.M., 2002. Hydrodynamic modelling of dense gas-fluidised beds: comparison of the kinetic theory of granular flow with 3-D hard-sphere discrete particle simulations. Chemical Engineering Science 57, 2059.

Hill, R.J., Koch, D.L., Ladd, A.J.C., 2001a. The first effects of fluid inertia on flow in ordered and random arrays of spheres. Journal of Fluid Mechanics 448, 213.

Hill, R.J., Koch, D.L., Ladd, A.J.C., 2001b. Moderate-Reynolds-number flows in ordered and random arrays of spheres. Journal of Fluid Mechanics 448, 243.

Hoomans, B.P.B., Kuipers, J.A.M., Briels, W.J., van Swaaij, W.P.M., 1996. Discrete particle simulation of bubble and slug formation in a two-dimensional gas-fluidized bed: a hard sphere approach. Chemical Engineering Science 51, 99.

Jenkins, J.T., Richman, M.W., 1988. Plane simple shear flow of smooth inelastic circular disks: the anisotropy of the second moment in the dilute and dense limits. Journal of Fluid Mechanics 192, 313.

Jenkins, J.T., Savage, S.B., 1983. A theory for the rapid flow of identical, smooth, nearly elastic particles. Journal of Fluid Mechanics 130, 187.

Kobayashi, N., Yamazaki, R., Mori, S., 2000. A study on the behavior of bubbles and solids in bubbling fluidized beds. Powder Technology 113, 327.

Kuipers, J.A.M., van Swaaij, W.P.M., 1998. Computational fluid dynamics applied to chemical reaction engineering. Advances in Chemical Engineering 24, 227.

Kuipers, J.A.M., van Duin, K.J., van Beckum, F.P.H., van Swaaij, W.P.M., 1992. A numerical model of gas-fluidized beds. Chemical Engineering Science 47, 1913.

Kuipers, J.A.M., Hoomans, B.P.B., van Swaaij, W.P.M., 1998. Hydrodynamic modeling of gas-fluidized beds and their role for design and operation of fluidized bed chemical reactors. Proceedings of the Fluidization IX Conference, Durango, USA. pp. 15–30.

Kunii, D., Levenspiel, O., 1991. Fluid Engineering. Butterworth Heinemann series in Chemical Engineering, London.

Ladd, A.J.C., 1993. Lattice-Boltzmann simulations of particle fluid suspensions. Journal of Fluid Mechanics 271, 285.

Ladd, A.J.C., Verberg, R., 2001. Lattice-Boltzmann simulations of particle fluid suspensions. Journal of Statistical Physics 104, 1191.

Li, J., Kuipers, J.A.M., 2003. Gas–particle interactions in dense gas-fluidized beds. Chemical Engineering Science 58, 711.

McNamara, G.R., Zanetti, G., 1988. Use of the Boltzmann equation to simulate lattice-gas automata. Physical Review Letters 61, 2332.

Nieuwland, J.J., Van Sint Annaland, M., Kuipers, J.A.M., van Swaaji, W.P.M., 1996. Hydrodynamic modeling of gas/particle flow in riser reactors. A.I.Ch.E. Journal 42, 1569.

Schiller, L., Nauman, A., 1935. A drag coefficient correlation. V.D.I. Zeitung 77, 318.

Succi, S., 2001. The Lattice Boltzmann Equation for Fluid Dynamics and Beyond. Oxford Science Publications, Clarendon Press, Oxford.

van der Hoef, M.A., Beetstra, R., Kuipers, J.A.M., 2004. Lattice Boltzmann simulations of low Reynolds number flow past mono- and bidisperse arrays of spheres: results for the permeability and drag force, submitted to the Journal of Fluid Mechanics.

van Swaaij, W.P.M., 1990. Chemical reactors. In: Davidson, J.F., Clift, R. (Eds.), Fluidization. Academic Press, London.

Walton, O.R., 1993. Numerical simulation of inelastic, frictional particle–particle interactions. In: Roco, M.C. (Ed.), Particulate Two-Phase Flow. Butterworth Heinemann series in Chemical Engineering, London.

Wen, C.Y., Yu, Y.H., 1966. Mechanics of fluidization. A.I.Ch.E. Series 62, 100.